Environmental Microbiology
October 2023, Volume 25, Issue 10, Pages 1816-1829
https://doi.org/10.1111/1462-2920.16397 https://archimer.ifremer.fr/doc/00836/94758/

Seasonal shifts in Fe-acquisition strategies in Southern Ocean microbial communities revealed by metagenomics and autonomous sampling

Zhang Rui [1], Debeljak Pavla [2, 3], Blain Stéphane [1], Obernosterer Ingrid [1, *]

[1] Sorbonne Université, CNRS, Laboratoire d'Océanographie Microbienne, LOMIC, Banyuls-sur-Mer, France
[2] Sorbonne Université, Muséum National d'Histoire, Naturelle, CNRS, EPHE, Université des Antilles, Institut de Systématique, Evolution, Biodiversité (ISYEB), Paris, France
[3] SupBiotech, Villejuif, France

* Corresponding author : Ingrid Obernosterer, email address : ingrid.obernosterer@obs-banyuls.fr

Abstract :

Iron (Fe) governs the cycling of organic carbon in large parts of the Southern Ocean. The strategies of diverse microbes to acquire the different chemical forms of Fe under seasonally changing organic carbon regimes remain, however, poorly understood. Here, we report high-resolution seasonal metagenomic observations from the region off Kerguelen Island (Indian Sector of the Southern Ocean) where natural Fe-fertilization induces consecutive spring and summer phytoplankton blooms. Our data illustrate pronounced, but distinct seasonal patterns in the abundance of genes implicated in the transport of different forms of Fe and organic substrates, of siderophore biosynthesis and carbohydrate-active enzymes. The seasonal dynamics suggest a temporal decoupling in the prokaryotic requirements of Fe and organic carbon during the spring phytoplankton bloom and a concerted access to these resources after the summer bloom. Taxonomic assignments revealed differences in the prokaryotic groups harbouring genes of a given Fe-related category and pronounced seasonal successions were observed. Using MAGs we could decipher the respective Fe- and organic substrate-related genes of individual taxa assigned to abundant groups. The ecological strategies related to Fe-acquisition provide insights on how this element could shape microbial community composition with potential implications on organic matter transformations in the Southern Ocean.

Originality Significance statement

The trace element iron is key for microbial metabolism, as a large number of enzymes involved in carbon-related pathways require iron as a co-factor. The acquisition of both elements is therefore essential for a cell to thrive in a given environment. Despite this key role of iron, the pathways used by diverse prokaryotes to access the different chemical forms of iron remains poorly understood. Understanding the iron acquisition strategies is of particular importance in marine environments where this trace element is present in growth-limiting concentrations. We report here high-resolution seasonal observations from a naturally iron-fertilized region in the Southern Ocean. Applying environmental metagenomics we identified different iron uptake strategies in marine prokaryotic communities and pronounced seasonal changes as an acclimation to varying iron and organic carbon regimes. Using metagenome-assembled genomes we further deciphered the Fe-related gene repertoire of individual taxa assigned to abundant prokaryotic groups. Our study provides novel insights to iron-related ecological strategies of diverse marine prokaryotes and how the acquisition of this element is linked to organic carbon.

Introduction

Organic carbon and iron (Fe) are essential elements for heterotrophic prokaryotes and from a metabolic point of view the two elements are intimately linked. Organic substrates provide building units for the cell and carbon metabolism is a source of energy, but a large number of enzymes involved in carbon-related pathways require Fe as a cofactor. The acquisition of both elements is therefore essential for a cell to thrive in a given environment. The concentration of marine organic matter varies on spatial and temporal scales and a large diversity of substrates with highly variable degrees of bioavailability make up this pool (Moran *et al.*, 2016). The concentration of inorganic nutrients can regulate the utilization of labile forms of organic matter, and Fe could be a rate-limiting micro-nutrient in High Nutrient Low Chlorophyll (HNLC) regions (Obernosterer *et al.*, 2015).

The marine Fe pool is made up by various dissolved and particulate forms originating from biological, lithogenic or authigenic sources (Tagliabue *et al.*, 2017), but the availability of these different forms of Fe to prokaryotes remains poorly investigated (Debeljak *et al.*, 2021; Hogle *et al.*, 2022; Manck *et al.*, 2022). The presence of multiple chemical forms of Fe is both a challenge and an opportunity for prokaryotes which have evolved a large panel of uptake strategies. Fe requirements and resource acquisition mechanisms vary among taxa (Hopkinson and Barbeau, 2012). *Roseobacter* genomes contain genes for multiple Fe uptake mechanisms, while SAR11 has a reduced set of transporters (Roe *et al.*, 2013; Hogle *et al.*, 2016). Siderophore biosynthesis appears to be restricted to a few prokaryotic groups, and many of these belong to *Gammaproteobacteria* (Hopkinson and Barbeau, 2012; Payne *et al.*, 2016; Manck *et al.*, 2022). By contrast, transporters of siderophore-bound Fe are more widespread (Hopkinson and Barbeau, 2012; Debeljak *et al.*, 2021; Hogle *et al.*, 2022), a differentiation that can lead to potential cross feeding (Cordero *et al.*, 2012). The prevalence of specific Fe uptake strategies was shown to be linked to Fe concentrations across large

77 spatial scales (Toulza *et al.*, 2012). Together, this results in a complex interplay between the
78 genomic and physiological properties of individual microbes and their interaction among
79 each other and with their micro-environment.
80 Responses of microbial communities from HNLC waters to additions of Fe and organic
81 carbon in short-term bottle incubation experiments largely depend on location and season
82 (Obernosterer *et al.*, 2015). While these experiments provide evidence that Fe and organic
83 carbon can constrain prokaryotic growth, they do not inform on potential acclimation of
84 microbes to changes in the supply of these elements. The aim of the present study was to
85 better understand the link between microbial Fe uptake strategies, organic matter supply and
86 microbial diversity in the Southern Ocean. Our specific objectives were firstly to determine
87 the seasonal dynamics in the functional repertoire of Fe- and organic substrate acquisition
88 genes and secondly to identify the microbial community members harboring these genes
89 under varying organic matter supply. We carried out our study in the region off Kerguelen
90 Island, a suitable environment because the intense spring and summer phytoplankton blooms
91 induced by natural Fe fertilization (Blain *et al.*, 2007) result in pronounced seasonal patterns
92 related to Fe and organic carbon availability. To address these objectives in an ocean region
93 that is difficult to access due to logistic constraints, we used an autonomous in situ sampler
94 providing high-resolution observations over an entire seasonal cycle.

Experimental Procedures

Sample collection

We used 12 seawater samples collected with a Remote Autonomous Sampler (RAS-500®, Mac Lane) from 25 October 2016 to 24 February 2017 in surface waters (40 m) of the Kerguelen plateau in the Indian sector of the Southern Ocean (Station A3, 527 m overall depth) (Figure 1). The technical aspects of the RAS and its mooring, and the collection of seawater are described in detail in Blain et al. (Blain *et al.*, 2021). Briefly, three samples (500 mL each) were collected at each time point; for inorganic nutrient analyses, one sample was filtered *in situ* through an 0.8 µm polycarbonate filter (PC, 47 mm diameter, Nuclepore, Whatman, Sigma-Aldrich, St Louis, MO), and for phytoplankton and prokaryotic diversity (Liu *et al.*, 2020; Blain *et al.*, 2021), two samples remained unfiltered. Fixatives (mercuric chloride or glutaraldehyde) were added to the sample bags prior to sampling. Upon recovery of the RAS, seawater for metagenomic analyses (fixed with mercuric chloride) was filtered sequentially through 0.8 and 0.2 µm PC filters (47 mm diameter, Nuclepore, Whatman, Sigma-Aldrich, St Louis, MO) and both filters were kept at -80 °C until DNA extraction. Only the DNA extracted from the 0.2 µm filters were used for metagenomic analyses. Temperature and salinity were obtained from sensors mounted on the RAS.

DNA extraction and metagenome sequencing

Total DNA was extracted from 0.2 µm PC filters using the DNeasy PowerWater Kit (Qiagen) according to the manufacturer's instructions with a few modifications. Each filter was cut into small pieces with the scissors, and added solution PW1 and incubated at 65°C for 10 min to promote cell lysis, the complete details of DNA extraction are given in the study by Liu et al. (Liu *et al.*, 2020). DNA concentration was measured using quantus fluorometer (Promega) with QuantiFluor® Double stranded DNA (dsDNA) system. Metagenome samples (n=12) were sequenced with an Illumina NovaSeq 6000 system using 2 × 150 bp chemistry at

Fasteris SA, Inc. (Switzerland), and yielded 59-83 Mio pairs of metagenomic reads per sample, corresponding to a total of 263.8 GB (Table S1). The data sets are available in the European Nucleotide Archive (ENA) repository at https://www.ebi.ac.uk/ena under the project ID PRJEB56376.

Metagenome assembly

The raw reads were checked with FastQC v0.11.9 and processed with Trimmomatic (v 0.32) (Bolger *et al.*, 2014). The short reads that passed the quality control (QC) were individually assembled by MEGAHIT v1.2.9 (Li *et al.*, 2015) (parameters used --presets meta-large). We also used metaSPAdes v3.14.1(Nurk *et al.*, 2017) (parameters used -k 21, 33, 55, 77, 99, 127) to assemble short reads for comparison. MetaQuast with default parameters was used to evaluate metagenomic assembly (Mikheenko *et al.*, 2016). For assembly using MEGAHIT, the total number of contigs varies between 0.1 and 1.6 Mio with an average length of 600 bp (Table S2). For the assembly using metaSPAdes, the total number of contigs varies between 0.3 and 1.8 Mio with an average length of 500 bp (Table S2). Due to the length of N50 we decided to continue the analysis from the MEGAHIT assembly results.

Metagenomic analysis

ORFs (open reading frames) were predicted using Prodigal v2.6.3 (Hyatt *et al.*, 2010) (parameters used -p meta) (Table S3). CD-HIT v4.8.1 (Li and Godzik, 2006) (parameters used -c 1 -aS 1 -g 1) was used to construct a non-redundant protein database pooling the twelve samples (10 984 076 proteins). Based on the non-redundant protein sequence number, we constructed the non-redundant gene sequence set. Salmon v1.4.0 (Patro *et al.*, 2017) was used for read recruitment of the short reads to the non-redundant gene sequences collection, and for the quantification of each gene in each sample (parameters used -incompatPrior 0.0 --seqBias --gcBias --biasSpeedSamp 5 -validateMappings). The quantified protein occurrences

144 for each sample were normalized as genes per kilobase million (GPM) using the following
145 formula:

146 $$GPM = 10^6 \times \frac{total\ reads\ mapped\ to\ genes/gene\ length\ in\ bp}{sum(total\ reads\ mapped\ to\ genes/gene\ length\ in\ bp)}$$

147 This value can be applied to the metagenomes to remove the effect of library size and gene
148 length, and GPM are thus comparable among samples.
149 To detect genes that are involved in Fe-related pathways, we used FeGenie (Garber *et al.*,
150 2020) based on individual contig files for alignment and annotation (parameters used --meta -
151 t 8 --norm). FeGenie is a bioinformatics tool to annotate iron-related genes by combining a
152 Hidden Markov Model (HMM) and BLAST. HMM is a probabilistic model used for gene
153 finding of sequencing data. The authors of FeGenie have constructed their own database of
154 HMMs for Fe related genes by obtaining HMMs from Pfam/TIGRFAMS or by manually
155 constructing HMMs. The HMMs were calibrated through queries against the NCBI's
156 database. Bit score cutoffs that optimally delineate between true and false positives among
157 hits from the non-redundant protein database were identified by manually inspecting each
158 hmm search result. In the present study we used this comprehensive library to identify
159 proteins that are related to Fe transport and storage, and siderophore biosynthesis and
160 transport (Table S4). The genes identified from the present dataset passed the recommended
161 bit score cutoffs. Different pathways can share homologous genes, as is the case for example
162 in siderophore biosynthesis. HMMs developed in FeGenie are sensitive to the entirety of each
163 gene family. In the metagenomes used here, not all domains of a given siderophore pathway
164 were detected at each time point (see Fig. S3). This is most likely due to the overall lower
165 GPMs of siderophore biosynthesis genes as compared to other Fe-related genes, and thus a
166 limit of detection at our sequencing depth. In order to obtain GPM for the identified FeGenie
167 proteins, each protein sequence related to the Fe pathway in each sample was retrieved in

fasta format and mapped against the non-redundant protein database using DIAMOND blastp. Proteins at 100% similarity were retrieved with the according GPM.

For the taxonomic affiliation of Fe-related genes, sequences were obtained using Centrifuge v1.0.4 (Kim *et al*., 2016) by searching against the GTDB database (Parks *et al*., 2022) and the alignments with highest score were kept. We then calculated the relative contribution of a prokaryotic group assigned to a gene of interest. The limitation of this approach is that taxonomy is assigned based on relatively short sequencing length of the individual genes; for this reason, we considered mainly the family level and used metagenome assembled genomes for a more resolutive description. Therefore, the GPM for each Fe-related gene in each sample were summed separately (corresponding to *a*), the GPM per taxa associated with each Fe-related gene in each sample were summed (corresponding to *b*), and the relative contribution of the prokaryotic group was calculated as *b*/*a*.

Organic substrate transporter annotation was carried out based on the non-redundant protein sequences set against TCDB (Saier, 2006) using DIAMOND blastp (parameters used --more-sensitive -e 1e-5), and amino acid similarity of ≥ 70% was chosen as threshold for further analysis. CAZymes were annotated based on the non-redundant protein sequences set using hmmsearch against the dbCAN database (e value < 1 × 10-10, coverage > 0.3) (Zhang *et al.*, 2018). The domain with the highest coverage was selected for sequences overlapping multiple CAZymes domains. The phylogenetic affiliation of organic substrate transporters and CAZymes sequences and the relative contribution of prokaryotic groups was determined using the same method as described above.

Visualization of data was performed using the packages ggplot2 in the R v4.0.3 and SigmaPlot v14.5 software. The heatmap was generated using the pheatmap package in the R v 4.0.3, with Euclidean distance as the distance function.

Analysis of Metagenome Assembled Genomes (MAG)

One MAG assigned to each SAR11 and *Nitrincolaceae*, and two MAGs assigned each to *Polaribacter* and *Rhodobacteraceae* were downloaded from data previously published by Sun et al. (Sun *et al.*, 2021). The seawater samples from which the MAGs were constructed were collected from 3 sites in the Kerguelen region including the study site of the RAS deployment. After sequencing, metagenomes were assembled and binned using the methods described by Sun et al.(Sun *et al.*, 2021). MAGs were reassessed using CheckM (v1.1.2) (Parks *et al.*, 2015) for completeness, and the completeness of the 6 MAGs used in the present study ranged from 55-94% (Table S5). The ANI values between MAGs, calculated using the OrthoANIu algorithm (Yoon *et al.*, 2017), were below 95%. ORFs of MAGs were predicted using Prodigal v2.6.3 (Hyatt *et al.*, 2010) (parameters used -p meta) and functional annotation of MAGs was carried out using the same method as above. To estimate the abundance of MAGs and their Fe- and organic substrate transporter and CAZymes-related genes across the twelve metagenomes, we first used Bowtie2 v2.4.4 (Langmead and Salzberg, 2012) with default parameters to recruit short reads from the twelve metagenomes and samtools (Li *et al.*, 2009) was used to convert the resulting SAM files into sorted and indexed BAM files. We used anvi'o v7.1 (Eren *et al.*, 2015) to profile short metagenomic reads aligned to MAGs to estimate coverage statistics per metagenome. Briefly, we first used the program 'anvi-gen-contigs-database' turning MAGs into a contigs-db, then used the program 'anvi-profile' to process the BAM file and generate individual anvi'o profile database, and used the program 'anvi-merge' to merge these individual profiles into a final merged profile database which stored the coverage statistics of each MAGs in the 12 metagenomes. Finally, the program 'anvi-summarize' generated mean coverage values of each MAG and each gene within them across the twelve metagenomes and was visualized by the program 'anvi-interactive' in 'gene mode'.

Results

Environmental context

The site of the RAS deployment is located southeast of Kerguelen Island in the Indian Sector of the Southern Ocean (Figure 1). This naturally Fe-fertilized region has been extensively studied during previous oceanographic cruises focusing on distinct time periods, that are early spring, mid and late summer (projects KEOPS1&2 and MOBYDICK). The deployment of the RAS from 25 October 2016 to 24 February 2017 has for the first time provided a full seasonal picture of the physical context (Pellichero *et al.*, 2020), inorganic nutrient concentrations and characteristics of the consecutive phytoplankton blooms and their carbon and trace element export (Blain *et al.*, 2021, 2022). Briefly, the spring phytoplankton bloom started in late October and peaked by mid-November and the summer bloom occurred in early January (Figure S1A). Diatoms dominated both blooms but varied considerably in their composition between seasons (Blain *et al.*, 2021). Surface water temperature steadily increased from 1.70°C to 4.17°C over the course of the sampling period. Concentrations of nitrate (range 21.95 to 27.69 µM) and silicic acid (range 2.45-8.24 µM) decreased during the observation period, while ammonium concentrations (range 0.3 to 2 µM) reached a maximum in late December (Figure S1B) (Blain *et al.*, 2021).

Seasonal trends in Fe and C transporters

In total 28 662 Fe-related genes were annotated in the FeGenie database, 66 005 genes related to substrate transport in the TCDB database and 136 460 genes related to enzymatic activity in the CAZymes database. Fe-related genes exhibited lowest normalized gene abundances (genes per kilobase million, GPM) (10-600 GPM), followed by organic carbon membrane transporters (600 to 1400 GPM) and CAZymes (7000 to 12000 GPM).

Normalized gene abundances (GPM) of each of these categories revealed pronounced seasonal patterns (Figure 2). Transporters of Fe ions (Fe^{3+}, Fe^{2+}) (Figure 2A), siderophores

242 and heme (Figure 2B) had the highest GPM after the blooms. Increases in GPM occurred
243 rapidly after the spring bloom and with a time lag of about one month after the summer
244 bloom. Siderophore biosynthesis genes had one peak during the spring bloom, and a second
245 peak after the summer bloom in parallel with various Fe transporters (Figure 2B). Organic
246 substrate transporters revealed the highest GPM during the spring bloom and a smaller peak
247 was observed one month after the summer bloom (Figure 2C). Organic substrate transporters
248 increased also during the final spring bloom decline, following the seasonal peak in
249 CAZymes.
250 The most abundant transporters of Fe^{3+} ions were *fbpABC*, *fut*A1/A2 and *fbpB-futB*, and the
251 dominant Fe^{2+} ion transporter genes were *feoAB* and *efeUOB* (Figure 3A) (Table S4).
252 Siderophore uptake genes were dominated by the *exbB-exbD-tonB* complex and among the
253 genes identified for the transport of specific siderophores were those of pyoverdin (*fpv*),
254 aerobactin (*hat*), ferric enterobactin (*pir*), ferripyochelin (*fpt*), and vibrioferrin (*pvu*) (Figure
255 3B). We further identified four siderophore biosynthesis clusters related to pyochelin (*pch*),
256 pyoverdin (*pvd*), rhizobactin (*rhb*) and vanchrobactin (*vab*) (Figures S2 and S3). Among
257 other Fe-related genes identified, a seasonal trend driven by the two phytoplankton blooms
258 was also detectable for Fe regulation (*fur*, *dtxR*, *fecR*), while genes for iron storage (*ftn*)
259 remained stable over time (Figure S2). Transporters of organic substrates were dominated by
260 those for amino acids and proteins, followed by sugars, glycerol and organic acids, and
261 transporters for vitamins were also present throughout the season (Figure 3C). During the
262 sampling period, 379 families of CAZymes were identified, among which 191 glycoside
263 hydrolase (GH) families, 82 glycosyltransferase (GT) families, 41 polysaccharide lyase (PL)
264 families, 34 carbohydrate-binding module (CBM) class families, 16 carbohydrate esterase
265 (CE) families and 13 auxiliary activities (AA) families (Figure 3D).
266 To obtain a more detailed picture of the seasonal patterns of genes involved in Fe and organic

substrate acquisition, we determined the similarity in the temporal trend among individual genes (Figure 4). This analysis highlights 4 periods. The first period, corresponding to the spring bloom (6 Nov and 17 Nov), was characterized by seasonally highest GPM of genes coding for siderophore synthesis (e.g., Pyochelin (*pch*), Pyoverdin (*pvd*), Vanchrobactin (*vab*)) and transport (e.g., catecholate receptor (*piu*), ferripyochelin (*fpt*), Vibriobactin (*viuB*)), concurrently with several organic substance transporters, such as amino acids, sugars, spermidine/putrescine, and sulfonates. During the second period, that corresponds to the immediately following decline of the spring bloom (28 Nov), concurrent peaks in transporters of Fe^{3+} ions (*fbp, fut*), heme (*hmu*) and siderophores (e.g., Vibrioferrin (*pvu*), Aerobactin (*hat*), Pyoverdin (*fpv*)) were observed. This period further revealed high GPM of several CAZymes (GT, CE, GH). The third period extends from the final declining phase of the spring bloom to the summer bloom (9, 20 and 31 Dec) and was characterized by enhanced GPM of transporters of Fe^{3+} ions (*fbpB-futB*, *futA1/A2*, *yfe*). The fourth period is represented by two sampling dates one month after the summer bloom (22 Jan and 2 Feb). Siderophore synthesis genes present already during the first phase re-emerged (e.g., *Pch*, *Pvd*, *Vab*) in combination with a new group of siderophore synthesis (e.g., Rhizobactin (*rhb*)) and transport (Ferric Enterobactin (*pir*), Legiobactin (*lbt*)) genes. During the fourth period, transporters of Fe peaked in parallel with those of organic compounds and siderophore synthesis genes, a pattern that contrasted our observations during the spring bloom.

Linking function to taxonomy at the family level

These temporal changes in the functional repertoire were paralleled by shifts in the prokaryotic community composition (Liu *et al.*, 2020) raising the question of the link between microbial diversity and Fe and organic substrate acquisition. To investigate whether the genes of interest were harbored by specific prokaryotic groups we assigned the taxonomy of the individual genes belonging to the different gene categories. We illustrate here the

taxonomic assignments of 4 genes, each representing the transport of a distinct form of Fe and each characterized by a marked seasonal trend; these are transport of Fe^{3+} ions (*fbp*) and Fe^{2+} ions (*feo*), of heme (*hmu*) and the siderophore ferric enterobactin receptor (*pir*) (Figure 5). The taxonomic assignments of other Fe-related genes are illustrated in Figure S4. The transporter *fbp* (Fe^{3+} ions) was assigned to several prokaryotic groups and their respective relative contributions changed considerably over time (Figure 5). During the spring bloom (period 1) when GPM were low, transport of Fe^{3+} ions was assigned to *Pseudomonadaceae*, *Pelagibacteraceae* and *Rhodobacteraceae*, while *Nitrincolaceae* dominated the taxonomic assignments (75 % of all *fbp* genes) when GPM peaked during the bloom decline (period 2). *Rhodobacteraceae* (in particular the genus *Amylibacter*, Figure S5) were the most abundant contributors to *fbp* (19-51%) during the remaining season and *Pseudomonadaceae* had an increasing share towards the end of the season (4-35%). A contrasting picture was obtained for *feo* (transport of Fe^{2+} ions) that was assigned to mainly two groups, *Sphingomonadaceae* in early spring (period 1) (28-39%) and *Flavobacteriaceae* throughout the remaining season (16-89%). *Flavobacteriaceae* were dominated by the genus *Polaribacter* (Figure S5) during the spring bloom decline (period 2). Heme uptake (*hmu*) revealed a seasonal abundance pattern similar to that of *fbp*, but had distinct taxonomic assignments. *Porticoccaceae* (7-43%), *Flavobacteriaceae* (2-76%) and *Nostocaceae* (2-14%) were the main contributors to heme uptake throughout the season. During the bloom decline (phase 2) when *hmu* peaked *Polaribacter irgensii* (*Flavobacteriaceae*) had a dominant contribution, and *Cellulophaga*, *hydrogenovibrio* and *Kordia* (*Flavobacteriaceae*) (Figure S5) prevailed over the remaining season. The ferric enterobactin receptor *pir* had a seasonal abundance pattern different to that of heme, with peaks during period 1 and 4, but overall similar taxonomic assignments at the family level. *Flavobacteriaceae* (6-66%), with substantial contributions of *Polaribacter*, *Pseudomonadaceae* and *Porticoccaceae* (1-13%) were the dominant contributors to *pir*, and

Sphingomonadaceae (0-15%) and *Cellvibrionacaea* (0-30%) had seasonally variable contributions. The taxonomic assignments of genes encoding for organic substrate transporters and CAZymes revealed overall small differences in the prokaryotic groups contributing to each category, but marked temporal changes in their relative contributions were observed, in particular during period 2 (Figures S6 and S7).

Genome-resolved functional potential

To obtain insights on the functional potential for the acquisition of both Fe and organic substrates, we used previously published metagenome assembled genomes (MAGs) obtained from samples collected in the Kerguelen region, including our study site (Sun *et al.*, 2021). We choose MAGs belonging to SAR11, *Nitrincolaceae*, *Rhodobacteracea*, and the genus *Polaribacter* (*Flavobacteriaceae*) (Figure 6 and Table S5). These MAGs belong to prokaryotic groups with substantial contributions to the different gene categories (Figure 5 and Figures S5-S7). Further, ASVs belonging to each of these groups were shown to be abundant and have pronounced seasonal relative abundance patterns, based on 16S rRNA gene sequencing from the same RAS deployment (Liu *et al.*, 2020). Mapping our metagenomic short reads to these MAGs revealed that they largely varied in their respective coverages and had each a distinct seasonal trend. SAR11 MAG133 had slightly higher coverage in early spring as compared to the remaining season. By contrast, *Nitrincolaceae* MAG115 revealed one sharp peak during period 2. The 2 *Rhodobacteraceae* MAGs had both higher coverage during the transition between the spring and summer blooms (period 3). By contrast, the 2 *Polaribacter* MAGs differed in their overall coverage and their seasonal dynamics. The inventories of the Fe- and organic substrate-acquisition genes provided some insights on the metabolic versatility of these MAGs. SAR11 MAG133 harbored a reduced set of Fe (*fut*, *fbp*B-*fut*B, Fe^{3+} ions) and organic substrate (sugars and amino acids) transporters. In *Nitrincolaceae* MAG115 we identified transporters for siderophore-bound Fe (*exbB-exbD*

342 complex and *fpv* for pyoverdin) and for several organic substrates (sugars, amino acids,
343 peptides) and vitamins. Both *Rhodobacteraceae* MAGs harbored transporters for Fe^{3+} ions
344 (*yfe*, *fbp*), but appear to differ in their potential of organic substrate acquisition. We identified
345 transporters of several substrates in *Rhodobacteraceae* MAG20 while only amino acid
346 transporters were detected in *Rhodobacteraceae* MAG52. Among the MAGs considered here,
347 *Polaribacter* MAG88 had the most diverse Fe-gene inventory, including heme and
348 bacterioferritin, absent from MAG64. The 2 *Polaribacter* MAGs harbored both transporters
349 of Fe^{2+} ions (*feo*), proteins and carboxylic acids.

Discussion

We observed pronounced seasonal patterns in the prevalence of genes for the transport of Fe and organic substrates by prokaryotic communities in the Southern Ocean. The acquisition of Fe was temporally decoupled from that of organic carbon over the course of the spring phytoplankton bloom, while a concerted access to both elements occurred after the summer bloom. These dynamics on the community level likely result from seasonal changes in the requirements of Fe and organic carbon and the functional capabilities to acquire the different chemical forms in which these elements are present by diverse microbial taxa. Using metagenome assembled genomes, we illustrate differences in the Fe- and organic substrate acquisition repertoires among abundant prokaryotic taxa. These observations combined with marked seasonal changes in microbial community composition (Liu *et al.*, 2020) provide new insights on the potential ecological niches of prokaryotes in the Fe- and organic carbon-constrained Southern Ocean.

Seasonal microbial response to phytoplankton blooms induced by natural iron fertilization

Natural Fe-fertilization in the region off Kerguelen Island leads to annually occurring phytoplankton blooms that impact ecosystem structure and functioning (Blain *et al.*, 2007). Heterotrophic prokaryotes respond markedly to these blooms in terms of growth, biomass production and respiration and thereby contribute to the processing of a substantial fraction of primary production during different seasons (Christaki *et al.*, 2021). The microbial communities present and active in these naturally Fe-fertilized waters vary over the course of the bloom (Liu *et al.*, 2020) and are distinct to communities in surrounding HNLC waters during different seasons (West *et al.*, 2008; Landa *et al.*, 2016; Hernandez-Magana *et al.*, 2021). Differences among prokaryotic taxa in Fe requirements and acquisition strategies as well as in the metabolic potential for the uptake of diverse phytoplankton-derived organic substrates could be one underlying mechanism (Teeling *et al.*, 2012; Debeljak *et al.*, 2019).

Niche differentiation in relation to Fe and organic carbon was recently described on a spatial scale (Sun *et al.*, 2021), but a temporal perspective is thus far lacking.

Microbial strategies and Fe sources during the spring bloom

The prevalence of organic substrate transporters during the spring bloom (period 1) points to a community that rapidly responds to the supply of labile phytoplankton-derived substrates. Organic carbon has been identified as a growth-limiting resource for the winter community in the Kerguelen region (Obernosterer *et al.*, 2015; Landa *et al.*, 2016). Our data suggest that amino acids, organic acids, sugars and sulfonates are the most prominent substances utilized, confirmed by metatranscriptomics and -proteomics data at the same study site (Debeljak *et al*., unpublished) and as reported previously from phytoplankton blooms in other marine environments (Teeling *et al.*, 2012; T. B. Francis *et al.*, 2021). The seasonal pattern of organic substrate transporters was, however, decoupled from that of Fe-transporters during the spring bloom, raising the question of how prokaryotes meet their Fe-requirements.

Dissolved Fe concentrations are high in surface waters in early spring (0.16 nM) (Quéroué *et al.*, 2015), but heterotrophic prokaryotes compete with fast growing small phytoplankton for this Fe source (Fourquez *et al.*, 2015). As reported for diverse members of this clade (Liu *et al.*, 2020; Dinasquet *et al.*, 2022) SAR11 MAG133 was abundant in early spring. The small streamlined genomes of SAR11 (Giovannoni, 2017) have reduced Fe-uptake repertoires (Hogle *et al.*, 2016), as observed also for SAR11 MAG133 (Fe^{3+} ion transporters *fut*, *fbp*B-*fut*B). Using MICRO-CARD-FISH, SAR11 accounted for about 25% of community Fe uptake, while the contribution to leucine uptake was 50% in early spring in fertilized and HNLC waters (Fourquez *et al.*, 2016), indicating an efficient organic substrate utilization even under conditions when access to Fe is constrained. Low Fe requirements and an efficient transport of Fe and organic substrates could be a strategy of SAR11 to take advantage of the pool of labile substrates supplied by phytoplankton.

Lithogenic particles present a potentially important source of Fe in early spring above the Kerguelen plateau (Blain *et al.*, 2022). This Fe source is geochemically complex and needs to be rendered biologically available via dissolution as for example through the binding to high affinity ligands (Kalinowski *et al.*, 2000). Among the strongest binding ligands are catecholate-type siderophores and particle-associated prokaryotes were shown to express the genes implicated in the respective biosynthesis pathways (Debeljak *et al.*, 2021). The prevalence of a catecholate-type siderophore receptor gene (*piu*) during spring indicates that this Fe source could in part account for the prokaryotic demand. Taxonomic assignments revealed that *Pseudomonadaceae* were the most prominent group harboring this receptor, an observation that supports previous findings on the role of this group in siderophore biosynthesis and uptake (Schalk *et al.*, 2020). An alternative strategy could be the utilization of an internal reservoir, such as Fe stored in specific proteins (bacterioferritin, Ftn) (Andrews *et al.*, 2003). This capacity was shown for strains belonging to *Pseudoalteromonas* (Mazzotta *et al.*, 2020) and several prokaryotic groups, in particular *Flavobacteriaceae*, *Halieaceae* and *Altermonadaceae* contributed to the expression of the respective genes above the Kerguelen plateau in early spring (Debeljak *et al.*, 2019). We identified the gene coding for ferritin in *Polaribacter* MAG88, which had increased coverage during spring, in contrast to *Polaribacter* MAG64 that lacked this gene and revealed enhanced coverage later in the season. These observations illustrate potential niche differentiation among closely related taxa. The utilization of internal Fe stored as ferritin by some taxa could be a possible mechanism for the apparent temporal decoupling in requirements of organic substrates and Fe.

Fe acquisition strategies during the spring bloom decline

Microbial gene inventories related to Fe and organic carbon transport drastically changed during the decline of the spring bloom (period 2). The prevalence of all CAZyme families

indicates the presence of a chemically different pool of organic matter and the need to cleave polysaccharides to access organic carbon (Teeling *et al.*, 2012). The synchronized enhancement in the GPM of different types of Fe-transporters, including those for Fe^{3+} and Fe^{2+} ions, Fe bound to siderophores (Vibrioferrin (*pvu*), Aerobactin (*hat*), Pyoverdin (*fpv*)) and heme suggest an increased prokaryotic Fe demand in response to the shift in the organic carbon regime during the phytoplankton bloom decline. In contrast to early spring, remineralization is a key process providing different sources of Fe to the system. Our observations allow us to provide insights into possible Fe and organic carbon related strategies of three bacterial groups with distinct abundance patterns.

Nitrincolaceae, represented by MAG115, rapidly responded to the bloom decline. The marked seasonal pattern of MAG115, reaching highest coverages of all MAGs considered here, matched the relative abundances of the respective ASVs as determined from 16S rRNA gene sequences (Liu *et al.*, 2020). *Nitrincolaceae* dominated the taxonomic assignments of transporters of Fe^{3+} ions (*fbp*) during the bloom decline and MAG115 harbored several siderophore uptake genes, such as pyoverdine (*fpv*), a siderophore containing catecholate and hydroxamate groups. MAG115 also contained a large repertoire of organic substrate transporters indicating its capacity in the uptake of various labile compounds (B. Francis *et al.*, 2021). The rapid response to a pulsed supply of organic carbon by taking advantage of its potential to utilize different forms of Fe suggests a copiotrophic metabolic strategy, and idea that is further supported by the concurrent expression both at the transcriptomic and proteomic level of genes related to Fe- and organic carbon transport by *Nitrincolaceae* MAG115 (Debeljak *et al*., unpublished).

Polaribacter MAG88 (*Flavobacteriaceae*) also responded to the bloom decline, but its coverage remained comparatively low. This MAG harbored a large repertoire of transporters for organic substrates and Fe, and among the latter we identified the heme transporter *hmu*.

Heme is a porphyrin-bound source of Fe that can account for a large fraction of cellular Fe concentrations in phytoplankton and can become a source to heterotrophs when cells are destroyed such as by viral lysis or grazing (Honey *et al.*, 2013). Utilization of heme was demonstrated experimentally for strains belonging to the *Roseobacter* clade (Roe *et al.*, 2013; Hogle *et al.*, 2017), but many other abundant microbial groups appear to lack heme transporters (Hogle *et al.*, 2017). In the present study, *Flavobacteriaceae* had a substantial share of the taxonomic assignments of heme transporters (*hmu*), in particular during the bloom decline. Our data suggest that members belonging to *Flavobacteriaceae* could use this source of Fe, to account for its requirements during the degradation of phytoplankton derived organic substances. This potential niche specialization could play an important role in large particles where access to this source of Fe is facilitated.

Both *Roseobacter* MAGs had increased coverage during the transition between the spring decline and summer bloom, matching observations of members of this clade at the ASVs level (Liu *et al.*, 2020). While functional Fe-profiles were overall similar for both MAGs, MAG20 appears to have a larger organic substrate repertoire than MAG52. An analysis of *Roseobacter* genomes revealed the presence of multiple and diverse pathways for the acquisition of inorganic and organically bound Fe and several copies of ABC transporters (Hogle *et al.*, 2016). This indicates that this group can make use of a variety of chemical forms of Fe, an idea that is supported by observations on the transcriptomic (Debeljak *et al.*, 2019, 2021) level. This versatility with respect to Fe transport let us hypothesize that specialization of organic substrate utilization could be the underlying mechanism for the similar seasonal patterns of the two *Roseobacter* MAGs.

Parallel Fe and C acquisition following the productive season

Despite the smaller magnitude of the summer phytoplankton bloom as compared to spring, the community functional repertoire markedly changed with a time lag of about 1 month,

contrasting the rapid response to the spring bloom. The late summer period is characterized by slightly higher concentrations of dissolved organic carbon and seasonally highest prokaryotic abundance (Christaki *et al.*, 2021; Hernandez-Magana *et al.*, 2021) and remineralization presents the main source of Fe (Blain *et al.*, 2008; Sarthou *et al.*, 2008). These environmental conditions could be favorable for the energetically costly biosynthesis of siderophores, supported by our observation of the diverse assemblage of genes for the acquisition of siderophore-bound Fe at the end of the season. Among these the gene of the siderophore receptor *pir* (ferric enterobactin receptor) was assigned to *Flavobacteriaceae*, and the two *Polaribacter* MAGs harbored both this gene. Many members of *Flavobacteriaceae*, including *Polaribacter*, are specialized in the degradation of complex compounds, such as polysaccharides (Xing *et al.*, 2015; Kappelmann *et al.*, 2019). Our results indicate that the concurrent access to organic substrates and siderophore-bound Fe could be a strategy that renders these taxa efficient degraders of organic matter in the Southern Ocean.

By considering transporters for different forms of Fe and organic carbon, two elements that were shown to constrain prokaryotic growth in the Southern Ocean, we provide insights on temporal dynamics in nutrient acquisition at the community level. The distinct seasonal patterns in Fe transporters with respect to those of organic substrates suggest that there could be a switch in nutrient requirements along the season. Our results extend the use of biomarker genes that have allowed to identify nutrient stress of specific microbial groups on spatial scales (Saito *et al.*, 2014; Garcia *et al.*, 2020; Ustick *et al.*, 2021). The taxon-specific genomic capacities to access the different chemical forms of Fe could be the basis for ecological niches and drive the observed changes in prokaryotic community composition (Liu *et al.*, 2020) as an acclimation to the supply of phytoplankton-derived organic matter in this naturally fertilized region of the Southern Ocean.

Author contributions

Rui Zhang, Pavla Debeljak, Stephane Blain and Ingrid Obernosterer designed the research. Bioinformatic analyses were performed by Rui Zhang. Rui Zhang and Ingrid Obernosterer wrote the first draft of the manuscript. All authors contributed to editing the manuscript.

Acknowledgements

We thank the team of the Technical Division of the Institute of the Sciences of the Universe (DT-INSU) for the design and construction of the mooring for the RAS. We thank the captains and the crews of the R/V Marion Dufresne for their support during the deployment and the recovery of the RAS. The project SOCLIM (Southern Ocean and Climate) was supported by the Climate Initiative of the BNP Paribas Foundation, the French Polar Institute (Institut Polaire Paul Emile Victor), and the French program LEFE-CYBER of the CNRS-INSU. We thank Yan Liu who carried out the DNA extraction. We thank the French Institute of Bioinformatics (IFB; https://www.france-bioinformatique.fr) for providing computing resources. We thank to the reviewers for their insightful comments on a previous version of this manuscript. This work is part of the PhD thesis of R.Z. supported by the China Scholarship Council (CSC; No. 202006220057).

Competing of interests

The authors declare no competing interests.

Data availability statement

The data sets generated and analysed during the current study are available in the European Nucleotide Archive (ENA) repository at https://www.ebi.ac.uk/ena under the project ID PRJEB56376.

References

Andrews, S.C., Robinson, A.K., and Rodríguez-Quiñones, F. (2003) Bacterial iron homeostasis. *FEMS Microbiol Rev* **27**: 215–237.

Blain, S., Planquette, H., Obernosterer, I., and Guéneuguès, A. (2022) Vertical Flux of Trace Elements Associated with Lithogenic and Biogenic Carrier Phases in the Southern Ocean. *Global Biogeochemical Cycles* **36**: 5.

Blain, S., Quéguiner, B., Armand, L., Belviso, S., Bombled, B., Bopp, L., et al. (2007) Effect of natural iron fertilization on carbon sequestration in the Southern Ocean. *Nature* **446**: 1070–1074.

Blain, S., Rembauville, M., Crispi, O., and Obernosterer, I. (2021) Synchronized autonomous sampling reveals coupled pulses of biomass and export of morphologically different diatoms in the Southern Ocean. *Limnology & Oceanography* **66**: 753–764.

Blain, S., Sarthou, G., and Laan, P. (2008) Distribution of dissolved iron during the natural iron-fertilization experiment KEOPS (Kerguelen Plateau, Southern Ocean). *Deep Sea Research Part II: Topical Studies in Oceanography* **55**: 594–605.

Bolger, A.M., Lohse, M., and Usadel, B. (2014) Trimmomatic: a flexible trimmer for Illumina sequence data. *Bioinformatics* **30**: 2114–2120.

Christaki, U., Gueneugues, A., Liu, Y., Blain, S., Catala, P., Colombet, J., et al. (2021) Seasonal microbial food web dynamics in contrasting Southern Ocean productivity regimes. *Limnol Oceanogr* **66**: 108–122.

Cordero, O.X., Ventouras, L.-A., DeLong, E.F., and Polz, M.F. (2012) Public good dynamics drive evolution of iron acquisition strategies in natural bacterioplankton populations. *Proc Natl Acad Sci USA* **109**: 20059–20064.

Debeljak, P., Blain, S., Bowie, A., Merwe, P., Bayer, B., and Obernosterer, I. (2021) Homeostasis drives intense microbial trace metal processing on marine particles. *Limnology & Oceanography* **66**: 3842–3855.

Debeljak, P., Toulza, E., Beier, S., Blain, S., and Obernosterer, I. (2019) Microbial iron metabolism as revealed by gene expression profiles in contrasted Southern Ocean regimes. *Environ Microbiol* **21**: 2360–2374.

Dinasquet, J., Landa, M., and Obernosterer, I. (2022) SAR11 clade microdiversity and activity during the early spring blooms off Kerguelen Island, Southern Ocean. *Environ Microbiol Rep* 1758-2229.13117.

Eren, A.M., Esen, Ö.C., Quince, C., Vineis, J.H., Morrison, H.G., Sogin, M.L., and Delmont, T.O. (2015) Anvi'o: an advanced analysis and visualization platform for 'omics data. *PeerJ* **3**: e1319.

Fourquez, M., Beier, S., Jongmans, E., Hunter, R., and Obernosterer, I. (2016) Uptake of Leucine, Chitin, and Iron by Prokaryotic Groups during Spring Phytoplankton Blooms Induced by Natural Iron Fertilization off Kerguelen Island (Southern Ocean). *Front Mar Sci* **3**.

Fourquez, M., Obernosterer, I., Davies, D.M., Trull, T.W., and Blain, S. (2015) Microbial iron uptake in the naturally fertilized waters in the vicinity of the Kerguelen Islands: phytoplankton–bacteria interactions. *Biogeosciences* **12**: 1893–1906.

Francis, B., Urich, T., Mikolasch, A., Teeling, H., and Amann, R. (2021) North Sea spring bloom-associated Gammaproteobacteria fill diverse heterotrophic niches. *Environmental Microbiome* **16**: 15.

Francis, T.B., Bartosik, D., Sura, T., Sichert, A., Hehemann, J.-H., Markert, S., et al. (2021) Changing expression patterns of TonB-dependent transporters suggest shifts in polysaccharide consumption over the course of a spring phytoplankton bloom. *ISME J* **15**: 2336–2350.

Garber, A.I., Nealson, K.H., Okamoto, A., McAllister, S.M., Chan, C.S., Barco, R.A., and Merino, N. (2020) FeGenie: A Comprehensive Tool for the Identification of Iron Genes and Iron Gene Neighborhoods in Genome and Metagenome Assemblies. *Front Microbiol* **11**: 37.

Garcia, C.A., Hagstrom, G.I., Larkin, A.A., Ustick, L.J., Levin, S.A., Lomas, M.W., and Martiny, A.C. (2020) Linking regional shifts in microbial genome adaptation with surface ocean biogeochemistry. *Phil Trans R Soc B* **375**: 20190254.

Giovannoni, S.J. (2017) SAR11 Bacteria: The Most Abundant Plankton in the Oceans. *Annu Rev Mar Sci* **9**: 231–255.

Hernandez-Magana, A.E., Liu, Y., Debeljak, P., Crispi, O., Marie, B., Koedooder, C., and Obernosterer, I. (2021) Prokaryotic diversity and activity in contrasting productivity regimes in late summer in the Kerguelen region (Southern Ocean). *Journal of Marine Systems* **221**: 103561.

Hogle, S.L., Brahamsha, B., and Barbeau, K.A. (2017) Direct Heme Uptake by Phytoplankton-Associated *Roseobacter* Bacteria. *mSystems* **2**: e00124-16.

Hogle, S.L., Hackl, T., Bundy, R.M., Park, J., Satinsky, B., Hiltunen, T., et al. (2022) Siderophores as an iron source for picocyanobacteria in deep chlorophyll maximum layers of the oligotrophic ocean. *ISME J* **16**: 1636–1646.

Hogle, S.L., Thrash, J.C., Dupont, C.L., and Barbeau, K.A. (2016) Trace Metal Acquisition by Marine Heterotrophic Bacterioplankton with Contrasting Trophic Strategies. *Appl Environ Microbiol* **82**: 1613–1624.

Honey, D., Gledhill, M., Bibby, T., Legiret, F., Pratt, N., Hickman, A., et al. (2013) Heme b in marine phytoplankton and particulate material from the North Atlantic Ocean. *Mar Ecol Prog Ser* **483**: 1–17.

Hopkinson, B.M. and Barbeau, K.A. (2012) Iron transporters in marine prokaryotic genomes and metagenomes: Iron transporters in marine prokaryotes. *Environmental Microbiology* **14**: 114–128.

Hyatt, D., Chen, G.-L., LoCascio, P.F., Land, M.L., Larimer, F.W., and Hauser, L.J. (2010) Prodigal: prokaryotic gene recognition and translation initiation site identification. *BMC Bioinformatics* **11**: 119.

Kalinowski, B.E., Liermann, L.J., Givens, S., and Brantley, S.L. (2000) Rates of bacteria-promoted solubilization of Fe from minerals: a review of problems and approaches. *Chemical Geology* **169**: 357–370.

Kappelmann, L., Krüger, K., Hehemann, J.-H., Harder, J., Markert, S., Unfried, F., et al. (2019) Polysaccharide utilization loci of North Sea Flavobacteriia as basis for using SusC/D-protein expression for predicting major phytoplankton glycans. *ISME J* **13**: 76–91.

Kim, D., Song, L., Breitwieser, F.P., and Salzberg, S.L. (2016) Centrifuge: rapid and sensitive classification of metagenomic sequences. *Genome Res* **26**: 1721–1729.

Landa, M., Blain, S., Christaki, U., Monchy, S., and Obernosterer, I. (2016) Shifts in bacterial community composition associated with increased carbon cycling in a mosaic of phytoplankton blooms. *ISME J* **10**: 39–50.

Langmead, B. and Salzberg, S.L. (2012) Fast gapped-read alignment with Bowtie 2. *Nat Methods* **9**: 357–359.

Li, D., Liu, C.-M., Luo, R., Sadakane, K., and Lam, T.-W. (2015) MEGAHIT: an ultra-fast single-node solution for large and complex metagenomics assembly via succinct de Bruijn graph. *Bioinformatics* **31**: 1674–1676.

Li, H., Handsaker, B., Wysoker, A., Fennell, T., Ruan, J., Homer, N., et al. (2009) The Sequence Alignment/Map format and SAMtools. *Bioinformatics* **25**: 2078–2079.

Li, W. and Godzik, A. (2006) Cd-hit: a fast program for clustering and comparing large sets of protein or nucleotide sequences. *Bioinformatics* **22**: 1658–1659.
Liu, Y., Blain, S., Crispi, O., Rembauville, M., and Obernosterer, I. (2020) Seasonal dynamics of prokaryotes and their associations with diatoms in the Southern Ocean as revealed by an autonomous sampler. *Environ Microbiol* **22**: 3968–3984.
Manck, L.E., Park, J., Tully, B.J., Poire, A.M., Bundy, R.M., Dupont, C.L., and Barbeau, K.A. (2022) Petrobactin, a siderophore produced by Alteromonas, mediates community iron acquisition in the global ocean. *ISME J* **16**: 358–369.
Mazzotta, M.G., McIlvin, M.R., and Saito, M.A. (2020) Characterization of the Fe metalloproteome of a ubiquitous marine heterotroph, *Pseudoalteromonas* (BB2-AT2): multiple bacterioferritin copies enable significant Fe storage. *Metallomics* **12**: 654–667.
Mikheenko, A., Saveliev, V., and Gurevich, A. (2016) MetaQUAST: evaluation of metagenome assemblies. *Bioinformatics* **32**: 1088–1090.
Moran, M.A., Kujawinski, E.B., Stubbins, A., Fatland, R., Aluwihare, L.I., Buchan, A., et al. (2016) Deciphering ocean carbon in a changing world. *Proc Natl Acad Sci USA* **113**: 3143–3151.
Nurk, S., Meleshko, D., Korobeynikov, A., and Pevzner, P.A. (2017) metaSPAdes: a new versatile metagenomic assembler. *Genome Res* **27**: 824–834.
Obernosterer, I., Fourquez, M., and Blain, S. (2015) Fe and C co-limitation of heterotrophic bacteria in the naturally fertilized region off the Kerguelen Islands. *Biogeosciences* **12**: 1983–1992.
Parks, D.H., Chuvochina, M., Rinke, C., Mussig, A.J., Chaumeil, P.-A., and Hugenholtz, P. (2022) GTDB: an ongoing census of bacterial and archaeal diversity through a phylogenetically consistent, rank normalized and complete genome-based taxonomy. *Nucleic Acids Research* **50**: D785–D794.
Parks, D.H., Imelfort, M., Skennerton, C.T., Hugenholtz, P., and Tyson, G.W. (2015) CheckM: assessing the quality of microbial genomes recovered from isolates, single cells, and metagenomes. *Genome Res* **25**: 1043–1055.
Patro, R., Duggal, G., Love, M.I., Irizarry, R.A., and Kingsford, C. (2017) Salmon provides fast and bias-aware quantification of transcript expression. *Nat Methods* **14**: 417–419.
Payne, S.M., Mey, A.R., and Wyckoff, E.E. (2016) Vibrio Iron Transport: Evolutionary Adaptation to Life in Multiple Environments. *Microbiol Mol Biol Rev* **80**: 69–90.
Pellichero, V., Boutin, J., Claustre, H., Merlivat, L., Sallée, J., and Blain, S. (2020) Relaxation of Wind Stress Drives the Abrupt Onset of Biological Carbon Uptake in the Kerguelen Bloom: A Multisensor Approach. *Geophys Res Lett* **47**: 9.
Quéroué, F., Sarthou, G., Planquette, H.F., Bucciarelli, E., Chever, F., van der Merwe, P., et al. (2015) High variability in dissolved iron concentrations in the vicinity of the Kerguelen Islands (Southern Ocean). *Biogeosciences* **12**: 3869–3883.
Roe, K.L., Hogle, S.L., and Barbeau, K.A. (2013) Utilization of Heme as an Iron Source by Marine Alphaproteobacteria in the Roseobacter Clade. *Appl Environ Microbiol* **79**: 5753–5762.
Saier, M.H. (2006) TCDB: the Transporter Classification Database for membrane transport protein analyses and information. *Nucleic Acids Research* **34**: D181–D186.
Saito, M.A., McIlvin, M.R., Moran, D.M., Goepfert, T.J., DiTullio, G.R., Post, A.F., and Lamborg, C.H. (2014) Multiple nutrient stresses at intersecting Pacific Ocean biomes detected by protein biomarkers. *Science* **345**: 1173–1177.
Sarthou, G., Vincent, D., Christaki, U., Obernosterer, I., Timmermans, K.R., and Brussaard, C.P.D. (2008) The fate of biogenic iron during a phytoplankton bloom induced by

natural fertilisation: Impact of copepod grazing. *Deep Sea Research Part II: Topical Studies in Oceanography* **55**: 734–751.

Schalk, I.J., Rigouin, C., and Godet, J. (2020) An overview of siderophore biosynthesis among fluorescent Pseudomonads and new insights into their complex cellular organization. *Environ Microbiol* **22**: 1447–1466.

Sun, Y., Debeljak, P., and Obernosterer, I. (2021) Microbial iron and carbon metabolism as revealed by taxonomy-specific functional diversity in the Southern Ocean. *ISME J* **15**: 2933–2946.

Tagliabue, A., Bowie, A.R., Boyd, P.W., Buck, K.N., Johnson, K.S., and Saito, M.A. (2017) The integral role of iron in ocean biogeochemistry. *Nature* **543**: 51–59.

Teeling, H., Fuchs, B.M., Becher, D., Klockow, C., Gardebrecht, A., Bennke, C.M., et al. (2012) Substrate-Controlled Succession of Marine Bacterioplankton Populations Induced by a Phytoplankton Bloom. *Science* **336**: 608–611.

Toulza, E., Tagliabue, A., Blain, S., and Piganeau, G. (2012) Analysis of the Global Ocean Sampling (GOS) Project for Trends in Iron Uptake by Surface Ocean Microbes. *PLoS ONE* **7**: e30931.

Ustick, L.J., Larkin, A.A., Garcia, C.A., Garcia, N.S., Brock, M.L., Lee, J.A., et al. (2021) Metagenomic analysis reveals global-scale patterns of ocean nutrient limitation. *Science* **372**: 287–291.

West, N.J., Obernosterer, I., Zemb, O., and Lebaron, P. (2008) Major differences of bacterial diversity and activity inside and outside of a natural iron-fertilized phytoplankton bloom in the Southern Ocean. *Environ Microbiol* **10**: 738–756.

Xing, P., Hahnke, R.L., Unfried, F., Markert, S., Huang, S., Barbeyron, T., et al. (2015) Niches of two polysaccharide-degrading Polaribacter isolates from the North Sea during a spring diatom bloom. *ISME J* **9**: 1410–1422.

Yoon, S.-H., Ha, S., Lim, J., Kwon, S., and Chun, J. (2017) A large-scale evaluation of algorithms to calculate average nucleotide identity. *Antonie van Leeuwenhoek* **110**: 1281–1286.

Zhang, H., Yohe, T., Huang, L., Entwistle, S., Wu, P., Yang, Z., et al. (2018) dbCAN2: a meta server for automated carbohydrate-active enzyme annotation. *Nucleic Acids Research* **46**: W95–W101.

Figure Legends

Figure 1. Map of the region around Kerguelen Island and location of the deployment of the remote autonomous sampler (white dot). Insert shows global position of Kerguelen Island as indicated by a square. Monthly composite of chlorophyll for November 2016. Modified from Blain et al. (Blain *et al.*, 2022).

Figure 2. A. Temporal changes of Chlorophyll a (green shaded area) and abundance of genes for Fe^{3+} and Fe^{2+} transporters (A), siderophore-bound Fe and heme transporters, and siderophore biosynthesis (B) and carbon substrate transporters and carbohydrate-active enzymes (CAZymes) (C). Normalized gene abundances are given in genes per kilobase million (GPM) (see Material and Methods for details).

Figure 3. Abundance of individual genes contributing to Fe^{3+} and Fe^{2+} transport (A), heme and siderophore transport (B), organic substrate transport (C) and carbohydrate-active enzymes (CAZymes, D) at the 12 time points. Transporters of fatty acids, lipoproteins, ammonia, exopolysaccharides, and urea are pooled as 'others'. CAZyme classes include auxiliary activities (AA), carbohydrate-binding modules (CBM), carbohydrate esterases (CE), cohesin, glycoside hydrolases (GH), glycosyltransferases (GT), polysaccharide lyases (PL), and S-layer homology domain (SLH). Normalized gene abundances are given in genes per kilobase million (GPM) (see Material and Methods for details).

Figure 4. Heatmap illustrates the seasonal patterns of genes involved in Fe and organic substrate transporters and related processes. Similarity between genes is based on Euclidian distance cluster analysis. Color intensity is determined by Z-score transformed normalized gene abundances (GPM). The vertical lines separate the four periods.

Figure 5. Temporal changes of normalized gene abundance (GPM) and relative contribution of prokaryotic groups to specific genes associated with Fe^{3+}, Fe^{2+}, heme and siderophore transport. Prokaryotic groups are based on the family level. Prokaryotic groups discussed in the text are marked in red.

Figure 6. Mean coverage of MAGs in the twelve samples and inventories of genes related to Fe and organic substrate transport and CAZymes. Mean coverage on the upper panel represents the average depth of coverage across contig (the coverage of each nucleotide in a contig divided by the length of the contig). Mean coverage on the lower panel represents the Σ coverage of each bp in a gene / gene length.

Figure 1

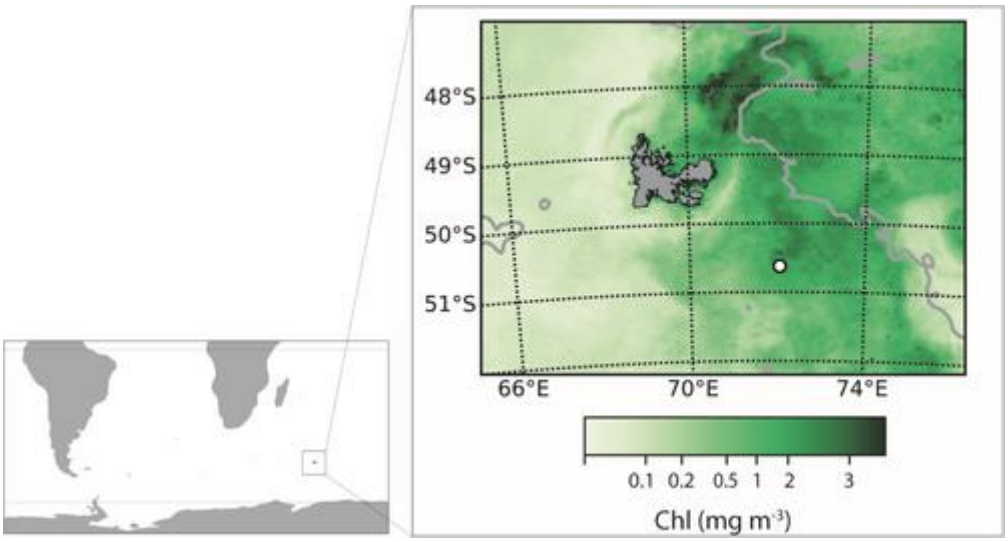

Figure 2

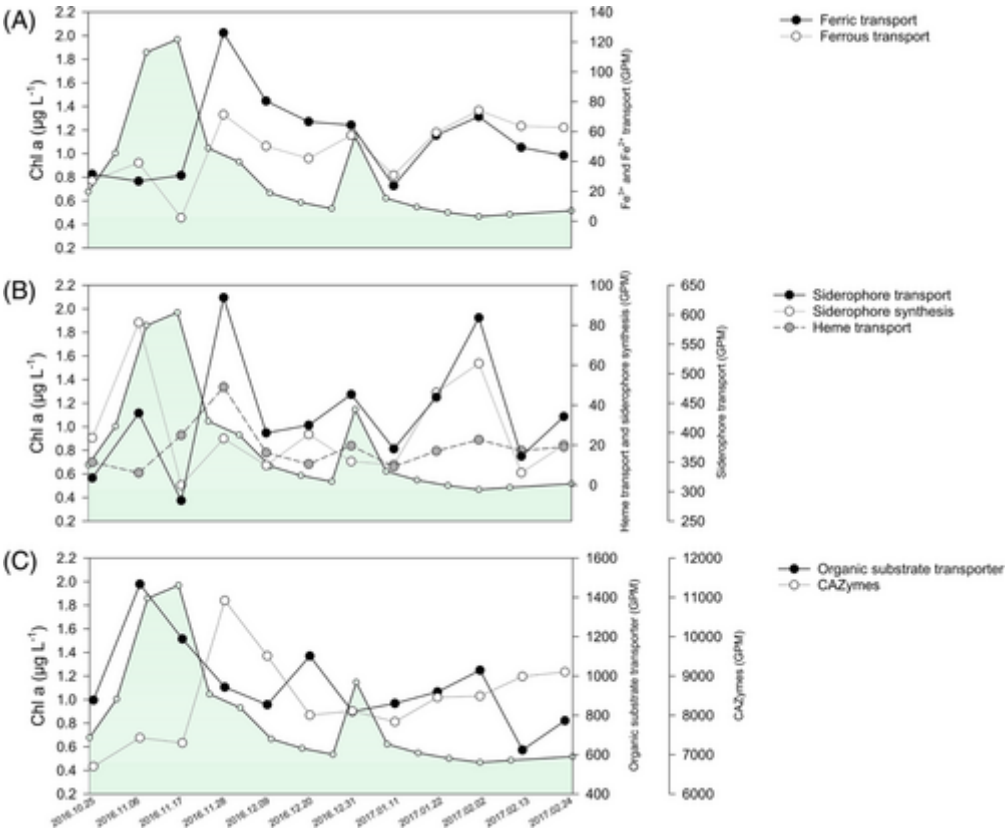

Figure 3

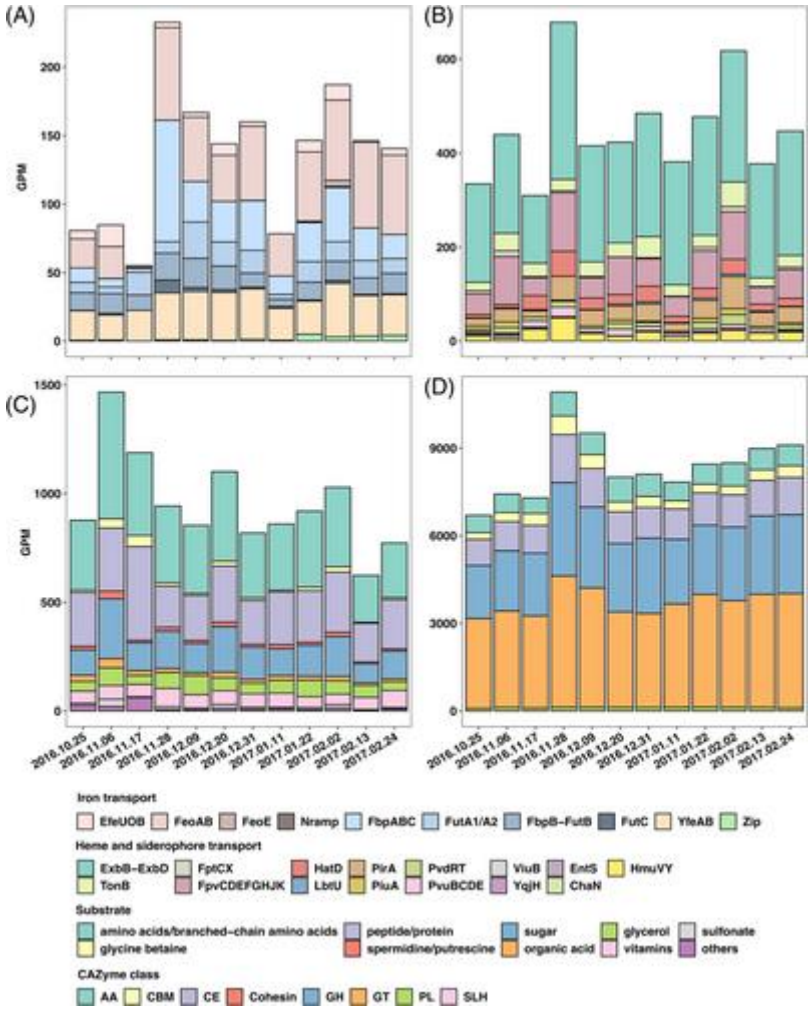
(A)
(B)
(C)
(D)
GPM
2016.10.25
2016.11.06
2016.11.17
2016.11.28
2016.12.09
2016.12.20
2016.12.31
2017.01.11
2017.01.22
2017.02.02
2017.02.13
2017.02.24
Iron transport
EfeUOB FeoAB FeoE Nramp FbpABC FutA1/A2 FbpB-FutB FutC YfeAB Zip
Heme and siderophore transport
ExbB-ExbD TonB FptCX FpvCDEFGHJK HatD LbtU PirA PiuA PvdRT PvuBCDE ViuB YqjH EntS ChaN HmuVY
Substrate
amino acids/branched-chain amino acids glycine betaine peptide/protein spermidine/putrescine sugar organic acid glycerol vitamins sulfonate others
CAZyme class
AA CBM CE Cohesin GH GT PL SLH

Figure 4

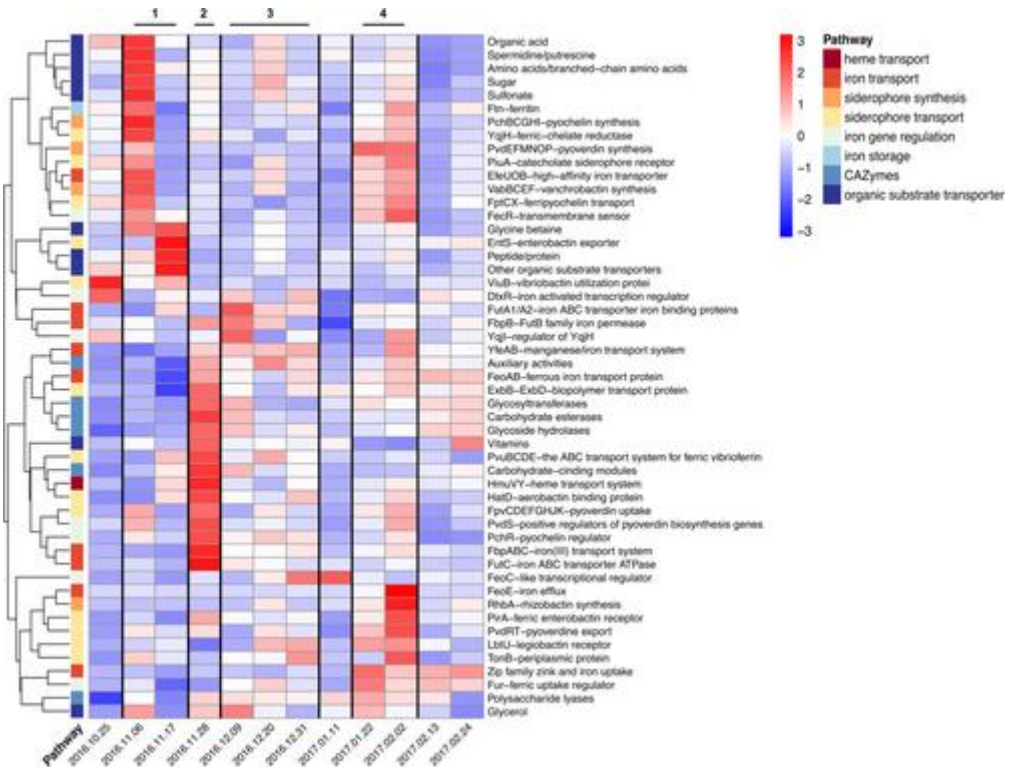

Figure 5

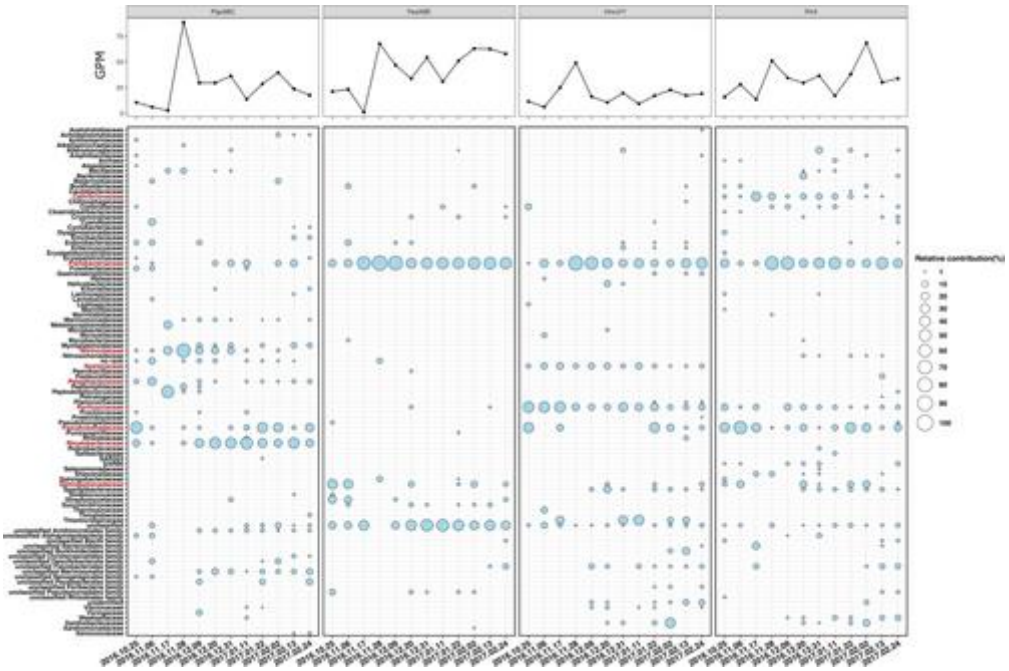

Figure 6

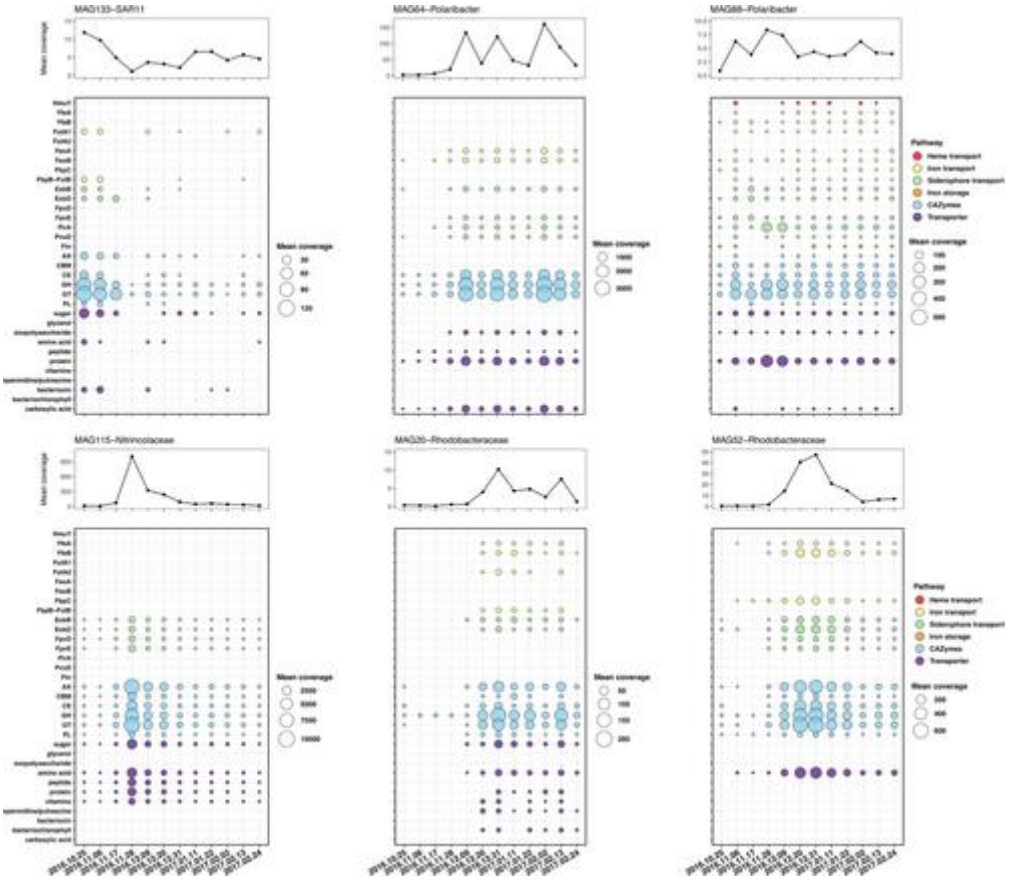
MAG133–SAR11
MAG64–Polaribacter
MAG88–Polaribacter
MAG115–Nitrincolaceae
MAG20–Rhodobacteraceae
MAG52–Rhodobacteraceae
Pathway
Heme transport
Iron transport
Siderophore transport
Iron storage
CAZymes
Transporter
Mean coverage